THE ASTROPHYSICAL JOURNAL, 225:655–664, 1978 October 15

THE SOLAR HYDROGEN LYMAN-β AND LYMAN-α LINES: DISK CENTER OBSERVATIONS FROM *OSO 8* COMPARED WITH THEORETICAL PROFILES

P. GOUTTEBROZE, P. LEMAIRE, J. C. VIAL, AND G. ARTZNER
Laboratoire de Physique Stellaire et Planétaire, Verrières-le-Buisson, France
Received 1978 March 6; accepted 1978 April 20

ABSTRACT

The solar Lα and Lβ lines of hydrogen have been measured at the center of the disk with the LPSP spectrometer aboard *OSO 8*. These line profiles are compared with theoretical profiles obtained with different solar atmospheric models, assuming either complete or partial frequency redistribution in scattering. The assumption of microturbulence for the velocity fields appears insufficient to account for the profiles of the line cores; better results are obtained with a blend of micro- and macroturbulence, which shows the need of a generalized treatment of the turbulent motions in the formation of these lines. If the effects of partial redistribution are taken into account, a good fit of the line wings requires higher temperatures, in the region under the plateau, than in the reference atmospheric model of Vernazza, Avrett, and Loeser.

Subject headings: line formation — line profiles — Sun: chromosphere — Sun: spectra — ultraviolet: spectra

I. INTRODUCTION

The solar lines of the Lyman series of hydrogen originate from the high chromosphere and are among the most appropriate tools for studying the structure of this part of the solar atmosphere. Although this paper is mainly devoted to Lβ, the same studies have been done simultaneously for Lα, which is the subject of a more abundant literature.

Since about 1962, photographic line profile observations of the Lβ line have been available (Tousey 1963; Tousey *et al.* 1964), and others were obtained more recently (Nicolas *et al.* 1976; Bruns *et al.* 1976). The first photoelectric profile measurements of this line were obtained by the LPSP instrument aboard *OSO 8*, during 1975 and 1976. We present here some of these observations at the center of the solar disk, with simultaneous observations of Lα.

Various theoretical studies of the hydrogen lines have been done, and we shall not quote them exhaustively. In particular, Cuny (1968) performed non-LTE computations of Lα, Lβ, and Hα with a three-level and continuum model atom. Vernazza (1972) and Vernazza, Avrett, and Loeser (1973) computed solar atmospheric models using multilevel atoms for hydrogen and a number of other elements. Milkey and Mihalas (1973) introduced partial redistribution into the computations, and Cannon (1976) considered multidimensional geometry and velocity fields. In this paper, we compute the line profiles corresponding to various atmospheric models, under several different assumptions. We do not propose a new model, but suggest some modifications to the current ones, in order to obtain better agreement with our observations.

II. OBSERVATIONS AND DATA REDUCTION

The LPSP instrumentation on board *OSO 8* is a multichannel high-resolution spectrometer coupled to a 16 cm aperture Cassegrainian telescope. A detailed description of the instrument is given by Artzner *et al.* (1977), and preliminary results have already been published (Bonnet *et al.* 1978).

The data used in this paper were recorded on 1976 August 19 at the quiet Sun center. The entrance slit of the spectrometer projects an area of 2″ × 120″ on the Sun, the spectral resolution achieved was 0.02 Å and 0.06 Å in Lα and Lβ, respectively, and the grating mechanism was scanning the lines by steps of 0.0083 Å and 0.0074 Å, respectively. Raw data obtained in the Lβ channel are taken with and without a MgF_2 filter in order to estimate the contribution of grating orders giving wavelengths higher than 1200 Å. The detailed techniques of data reduction are described in Lemaire *et al.* (1978). Lα and Lβ profiles are filtered from noise and restored from instrumental profile by using Fourier transform techniques as described by Brault and White (1971).

In order to obtain the absolute intensities of profiles, an absolute flux measurement was made during a rocket flight on 1976 February 18 (Lemaire *et al.* 1978). The Lα and Lβ fluxes at Earth, integrated over the profile are (5.4 ± 1.6) and (0.078 ± 0.019) ergs $cm^{-2}\,s^{-1}$, respectively. Calibrated profiles are given

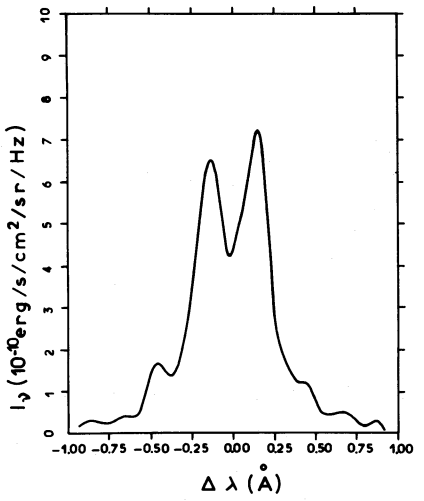

FIG. 1a

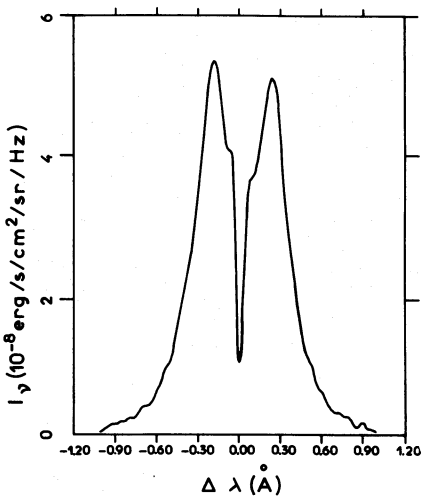

FIG. 1b

FIG. 1.—Observed profiles at the center of the solar disk. (*a*) Lβ. (*b*) Lα.

on Figure 1. The half-profiles obtained by symmetrization of these profiles are used in the next sections as a reference for computation.

III. THE ATMOSPHERIC MODELS

The models of the solar atmosphere used here are in hydrostatic equilibrium, including the effects of microturbulent pressure. The depth variable used to specify these models is the number (n_H) of hydrogen atoms (ionized or not) per cm^2 integrated along a vertical line. For convenience, the origin is not taken at infinity, but in an arbitrary point located in the near corona. Each model is essentially defined by the variation of the electronic temperature T_e as a function of n_H. The mean microturbulent velocity is given as a function of the geometrical depth z; this variation is the same for all models and is plotted on Figure 2. Up to 2400 km, this function is taken from Vernazza *et al.*; from there to 5000 km, the curve fits the mean slope of the eclipse observations reported by Hirayama (1971). The other data involved in the hydrostatic equilibrium are the gravity ($\log_{10} g = 4.44$), the pressure at the top of the atmosphere ($p_0 = 0.1$ dyne cm^{-2} in this work), and the abundances of elements, which are taken from the Harvard-Smithsonian Reference Atmosphere (Gingerich *et al.* 1971).

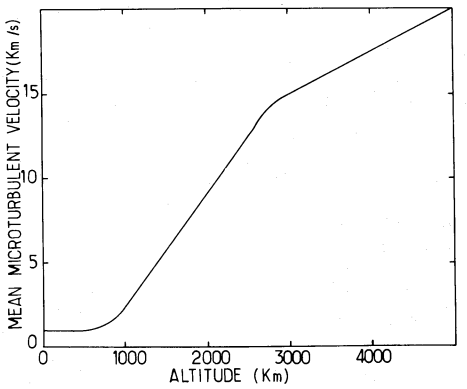

FIG. 2.—Mean microturbulent velocity versus altitude (model used in computations).

The total pressure is the sum of the atomic, electronic, and microturbulent pressures:

$$P = N_A kT_e + N_e kT_e + \tfrac{1}{2}\rho v_T^2 . \quad (1)$$

(N_A and N_e are the number densities of atoms and electrons; the other symbols have their usual meanings.)

A_i and m_i being, respectively, the abundance, relative to hydrogen, and the mass of the atom of the ith element, we define the following constants:

$$c_1 = \sum_i A_i m_i ,$$

and

$$c_2 = \sum_i A_i .$$

If η is the ratio of the electronic to the hydrogen density,

$$\eta = \frac{N_e}{N_H} , \quad \text{with } N_H = \frac{dn_H}{dz} , \quad \text{we have}$$

$$P = N_H(kT_e(c_2 + \eta) + \tfrac{1}{2}c_1 v_T^2) . \quad (2)$$

On the other hand, the equation of hydrostatic equilibrium may be written in the form

$$dP = \rho g dz ,$$

or

$$dP = c_1 g dn_H . \quad (3)$$

By combining the equations (2) and (3), we may obtain the following relation:

$$z - z_0 = \int_{n_H(z_0)}^{n_H} \frac{(c_2 + \eta)kT + \frac{1}{2}c_1 v_T^2}{c_1 g x + P_0}\, dx . \quad (4)$$

Given an initial set of z and η values, we may obtain a set of v_T values, using the function plotted on Figure 2, and compute a new set of z values by numerical integration of equation (4). A few iterations are necessary to achieve convergence. In this way, we obtain, with the geometrical depths, the hydrogen and electron densities needed for the line profile computations.

During the same time, η is computed by solving the ionization equilibrium equations for the main constituents of the solar atmosphere. We used the LTE ionization ratios for every element except hydrogen. In this case, the ratio $(N_{H\,II}/N_{H\,I})$ is computed for every value of n_H, by solving the statistical equilibrium equations for the hydrogen atom. The photoionization parameters are deduced from a prescribed set of radiation temperatures for the hydrogen bound-free transitions. These radiation temperatures are recomputed with the hydrogen lines and continua in another program which solves the radiative transfer and statistical equilibrium equations (see § IV). If the new radiation temperatures differ significantly from the previous ones, some iterations are done with the two programs in order to achieve consistency.

For the needs of computation, we considered only microturbulent velocities, although it is probably a poor approximation, especially in the upper chromosphere; it is also uncertain whether the general turbulence may be reduced to a superposition of micro- and macroturbulence, but it is probably a better approximation from the point of view of line profiles (this will be discussed in § V).

IV. COMPUTATION OF THE HYDROGEN LINE PROFILES

For each of the atmospheric models computed in the last section, we obtained the profiles of the hydrogen lines by solving simultaneously the equations of statistical equilibrium and radiative transfer for this atom. The radiative transfer equations for lines are solved by using a difference equation scheme (Feautrier's method) to obtain the intensities as functions of frequency and depth. This method has been extensively described in the literature (see, for instance, Feautrier 1964; Cuny 1967; Mihalas 1970), so we shall not reproduce it here. In this work, some computations were done by assuming partial redistribution in frequencies, others by assuming complete redistribution; a different program was used in each case.

The hydrogen bound-free transitions also were solved in a non–LTE way. For the Lyman continuum, we used a difference equation method similar to that used for the lines. For the other continua, which are less important for the determination of the statistical equilibrium, we used photoionization rates computed from a set of radiation temperatures deduced from the data of Makarova and Kharitonov (1969).

The statistical equilibrium equations were solved in the same way as in a previous work on the Mg II resonance lines (Gouttebroze 1977), and the iteration scheme between transfer and equilibrium equations is basically the same: from an initial set of radiative transition rates ("net radiative brackets" for the line and radiation temperatures for the continua), we compute the population of levels corresponding to the statistical equilibrium equations. We then execute several iterations to solve the radiative-transfer equation for the Lyman continuum, which gives new photoionization rates, and recompute the statistical equilibrium populations of levels corresponding to these rates. After that, some iterations are done to solve the radiative-transfer equations for the lines, and the populations are computed once more. This iteration scheme for the continuum and the lines is repeated several times. When the convergence is achieved, we obtain new values of the ionization ratio η; if the new values differ significantly from the starting values, the atmospheric model is recomputed as shown in § III.

Since the atomic parameters for hydrogen are generally well known, we simply used the values tabulated by Vernazza (1972), and did not check the effect of a change in these parameters, except for the collision-broadening parameters for Lα and Lβ, which are generally weaker than the natural broadening parameters but have an importance in specifying the ratio of coherent to incoherent scattering in the Omont-Smith-Cooper approximation (Omont, Smith, and Cooper 1972, hereafter OSC) (see Appendix). Two models of atoms were used. The first had five levels and a continuum. The intensities in the 10 lines and the Lyman continuum were computed in a self-consistent way, but prescribed to the observed values for the upper continua; the scattering was assumed to be completely redistributed in each line. To check the effects of partial redistribution, we used, for computational reasons of time and storage, a three-level and continuum model. The consequences of the limitation of the number of levels are not drastic, as will be shown in the next section. We considered only the effects of partial redistribution inside of the Lα and Lβ lines, in the approximation of OSC. For the Hα line, we continued to assume complete redistribution, because we were not interested in the determination of the profile of this line and, in addition, the actual redistribution function for Hα is rather complicated.

V. RESULTS FOR THE HYDROGEN LINES ALONE

As explained in § III, the following atmospheric models are specified by the variation of T_e versus n_H. As a reference model (labeled A), we used a distribution corresponding to the photosphere and chromosphere of Vernazza *et al.* (1973) with addition of the chromosphere-corona transition region of Jordan (1975) as reported by Avrett *et al.* This variation is plotted on Figure 3*a* (as said previously, the origin of n_H is arbitrary). The specification of the structure of

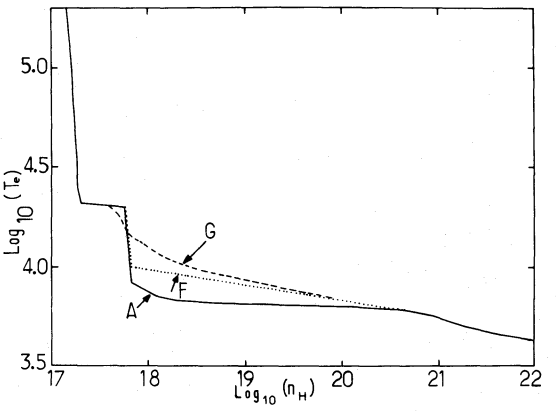

FIG. 3a

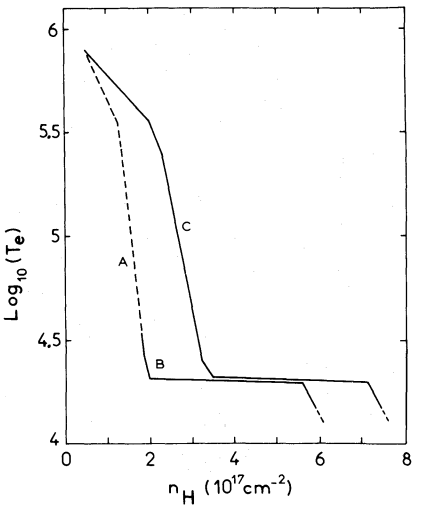

FIG. 3b

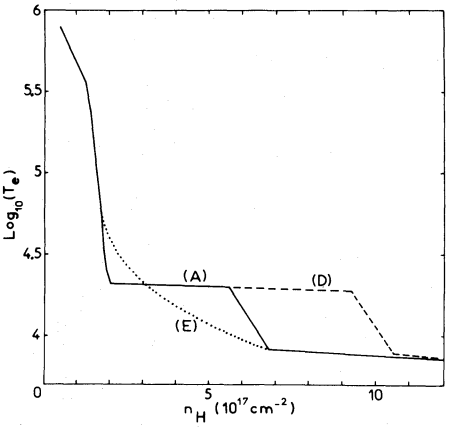

FIG. 3c

FIG. 3.—Electronic temperatures versus n_H for our seven atmospheric models. (*a*) Models A, F, and G (whole chromosphere). (*b*) Models A, B, and C (transition region). (*c*) Models A, D, and E (plateau).

the transition region, though not essential for the computation of the Lyman lines because hydrogen is almost completely ionized, has an influence on the central parts of these lines. Starting from this model, we tried a set of local modifications to see the contribution of various parts of the atmosphere to the emergent profile and seek a better fit to the observations. The influences of partial coherency in scattering and macroturbulence were neglected in a first step. They are studied in the following steps.

a) Five-Level and Continuum Atom with Complete Redistribution

The Lβ profile emitted by model atmosphere A differs from the observations by the sharpness of the peaks, and the intensities decrease much faster in the wings (Fig. 4*a*).

We first examined the influence of the thickness of the transition region on the Lβ profile. Model B corresponds to the atmosphere of Vernazza *et al.*, i.e., differs from A by the suppression of the transition region; C is similar to A, but the thickness of the transition region is increased by a factor of 2 (Fig. 3*b*). The resulting profiles are plotted on Figure 4*a*. The intensity at the center of the Lβ line increases with the thickness of the transition region, which contributes to the emission in the spectral range between the two peaks; the other parts of the profile remain practically unchanged.

In a similar way, the thickness of the plateau under the transition region was checked by using models D and E. In model D, the plateau is twice as thick, in n_H units, as the corresponding one in model A. The plateau is replaced, in model E, by a smoother curve between the middle chromosphere and the transition region (Fig. 3*c*). Model D increases the intensity in the peaks and broadens them; the other parts of the profile are less affected. With model E, the peaks disappear, and we obtain an emission profile without

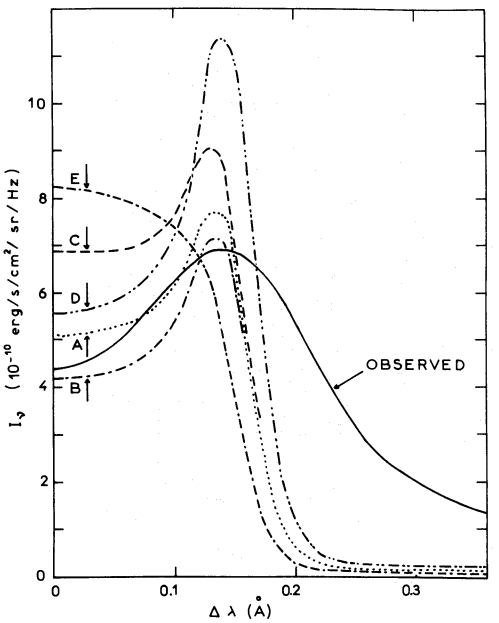

FIG. 4a

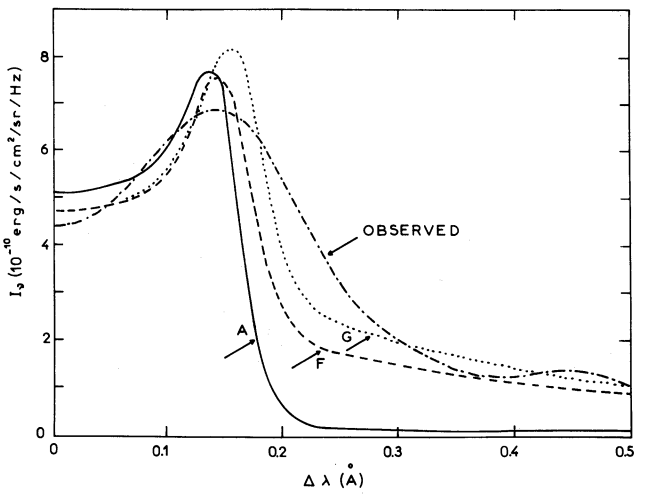

FIG. 4b

FIG. 4.—Lβ half-profiles obtained with five levels plus continuum computations, and complete redistribution. (*a*) Results for A, B, C, D, and E. (*b*) Results for A, F, and G.

reversal; this property of Lβ was first pointed out by Cuny (1968). In short, the intensity in the peaks depends mainly on the thickness of the plateau (Fig. 4*a*).

With model F, we sought the effect of an increase in the temperatures of the atmospheric region located under the plateau (Fig. 3*a*). The increase of temperatures in this region produces higher intensities in the near wings (Fig. 4*b*).

We continued to increase the temperature in order to obtain a better fit to the observed profile between 0.2 and 0.4 Å from line center; smoothing the transition with the plateau, we obtained in this way the atmospheric model G. The resulting Lβ profile is plotted on Figure 4*b* with other computed profiles and observations.

Now, let us consider the corresponding Lα profiles. With model A, we obtain the same kind of difference with the observed profiles as for Lβ: the emergent intensities at line center are too low (if we eliminate from the observations the narrow central absorption feature due to geocoronal hydrogen) and the peaks too high and narrow, and the intensity decreases too fast in the near wings (see Fig. 5*a*). An increase in the thickness of the transition region gives higher emission in the frequency range between the peaks, but this effect is weaker than in the case of Lβ (Fig. 5*a*). The comparison of the profiles given by models A, D, and E (Fig. 5*a*) shows that the intensity in the peaks of Lα is related, as is Lβ, with the thickness of the plateau; but in this case, the reversal does not disappear with model E. With models F and G, we obtain intensities which are too high in the near wings (Fig. 5*b*), but this discrepancy disappears when we take into account partial redistribution, as will be shown later.

b) *Three-Level and Continuum Atom with Partial Redistribution* (PRD)

The preceding profiles were computed under the assumption of complete redistribution of frequencies in scattering (CRD). If the intensities obtained for the central parts of the profiles (including the peaks) remain practically unaffected when we introduce partial coherency in scattering, the wings of the line are depressed. In the far wings, the observations become less accurate by reason of the fast decrease of the intensities, so that we limited our comparisons, in this work, to about 0.5 Å from line center for Lβ and 1 Å for Lα. Our model atom being restricted, in this case, to three levels and a continuum, we performed first the computations with CRD to see the effects of the limitation of the number of levels. On Figures 6*a* and 6*b* are plotted the profiles obtained with the reference model A, for Lβ and Lα, respectively. For Lβ, the intensities are lower in the case of three levels (by about 20% or less), but the shape of the profile remains the same; for Lα, the limitation of the number of levels has negligible effects. On the same figures, one may see the effects of PRD (in the OSC approximation): the core of the line is practically unchanged, but the wings are depressed, as was pointed out by Milkey and Mihalas (1973) for Lα. Since the effect of PRD on the line cores is very weak, we shall not give the results for models B to E, but consider

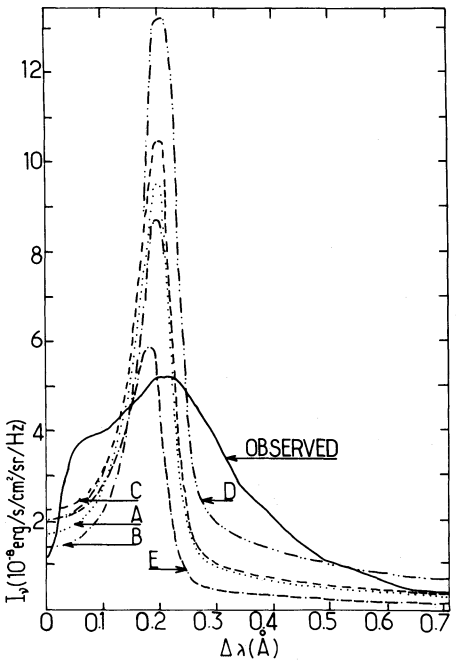

FIG. 5a

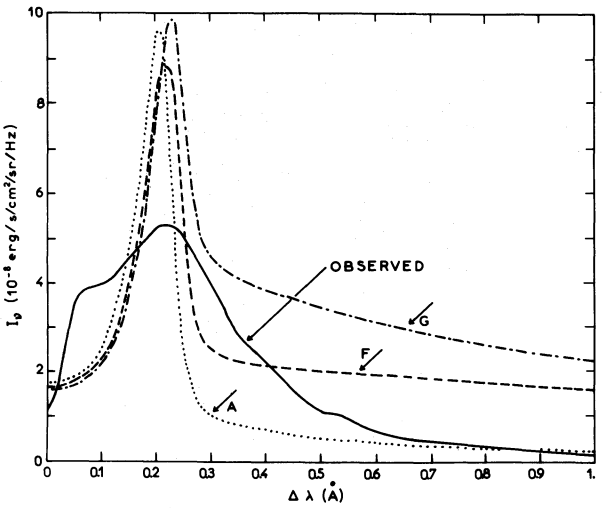

FIG. 5b

FIG. 5.—Lα half-profiles obtained with five levels and continuum computations, and complete redistribution

directly F and G. For Lα (Fig. 7*b*), the intensities in the wings decrease faster in the case of PRD than in the case of CRD; for this line, the collision-broadening parameters are lower than the natural ones, so that the scattering is essentially coherent in the wings. For the two atmospheric models, the PRD near wings fit the observations satisfactorily, while CRD wings are too high. For Lβ (Fig. 7*a*), the intensities in the PRD wings decrease faster than in the CRD wings, as for Lα, but the difference is smaller, the elastic collisions giving a substantial amount of incoherent scattering (see Appendix). For the two atmospheric models, the intensities in the near wings are in agreement with observations, except for the secondary peak of the observed profile between 0.4 and 0.5 Å, which may be attributed to the He II line (see § VI). This comparison between observed and computed profiles suggests that the temperature gradient between the plateau and the low chromosphere is not as steep as in the reference model A. Nevertheless, the wavelength range (1 Å)

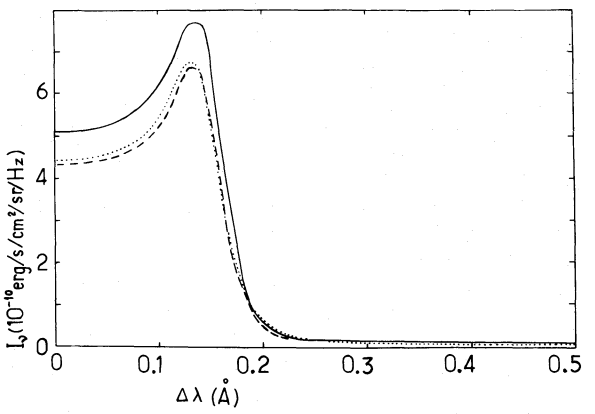

FIG. 6a

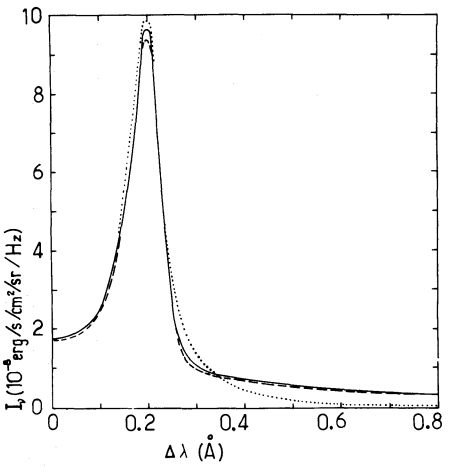

FIG. 6b

FIG. 6.—Effects of redistribution (partial or complete) obtained for model A. *Full line*, five levels and CRD; *dashed line*, three levels and CRD; *dotted line*, three levels and PRD. (*a*) Lβ. (*b*) Lα.

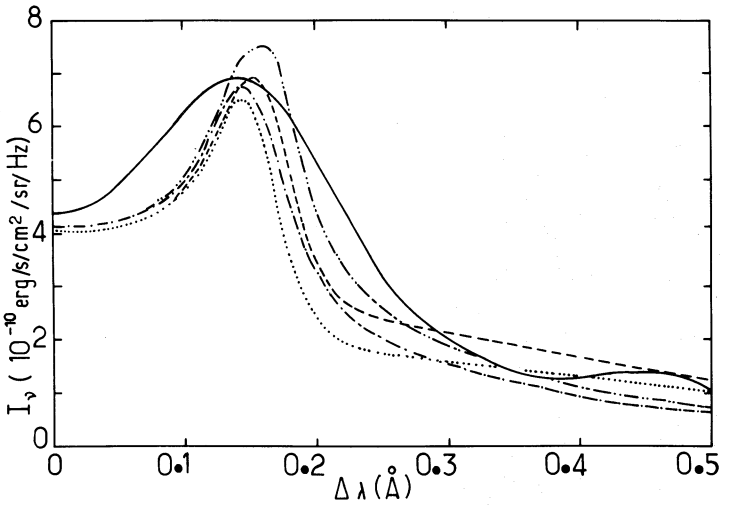

FIG. 7a

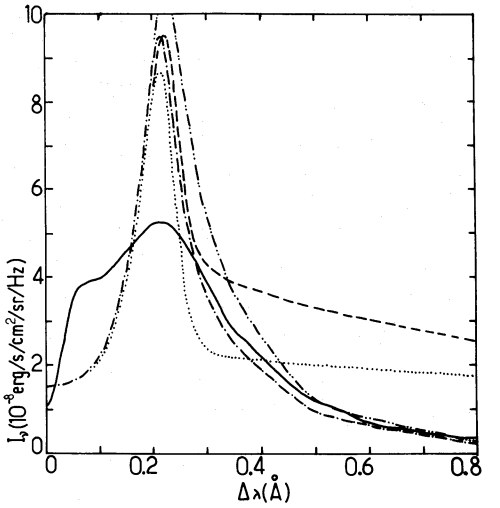

FIG. 7b

FIG. 7.—Effects of redistribution for models F and G. *Full line*, observations; *dotted line*, model F with CRD; *dashed line*, model G with CRD; *dot-dashed line*, model F with PRD; *dashed line with double dots*, model G with PRD. (*a*) Lβ. (*b*) Lα.

used for this comparison is too short to allow for the determination of the temperatures in this region. In this respect, models F and G, used for the sake of illustration, should not be considered as new reference models.

c) *Effects of Turbulence*

The above computations were done by assuming that the general turbulent motions of the solar atmosphere might be treated as microturbulence. Actually, the nature of the motions referred to as turbulent is not well known. Computations of the hydrogen lines with general turbulent motions are beyond the scope of this study.

However, one may try to approximate these motions by a superposition of the two limiting cases, micro- and macroturbulence. Vernazza (1972) showed that some discrepancies between the observations of the Lyman lines and the profiles computed with his model atmosphere may be reduced by adding macroturbulent motions with a rms velocity of 10 km s^{-1}.

As a convolution, the addition of macroturbulence acts primarily on the parts of the profile where the slope is steep. It may explain the fact that the observed

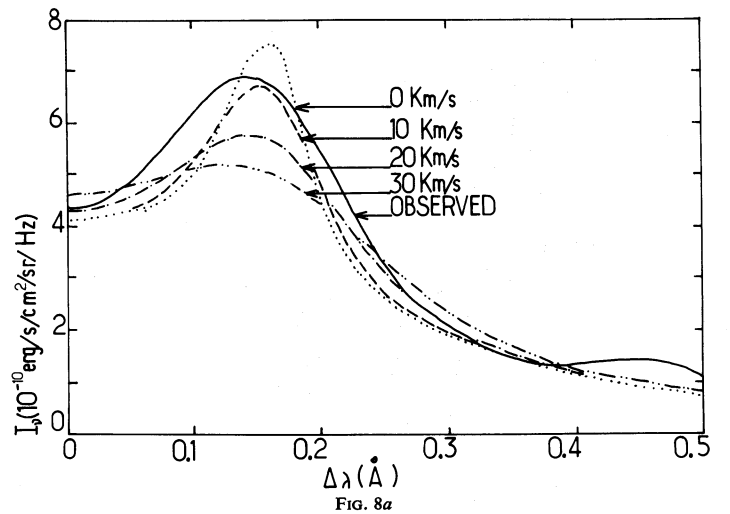

FIG. 8a

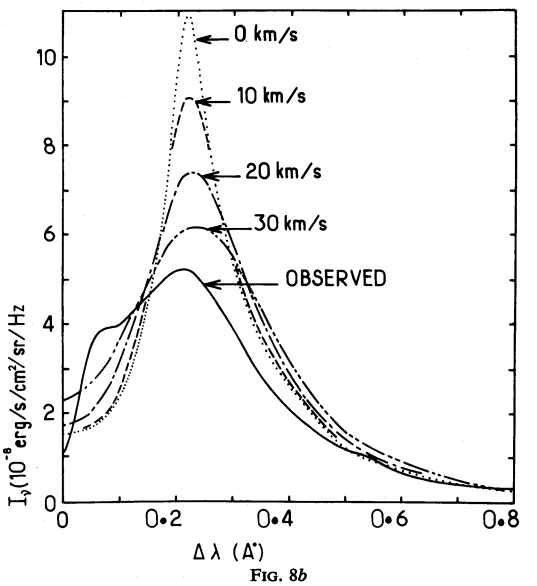

FIG. 8b

FIG. 8.—Effects of macroturbulent motions with rms velocities of 0, 10, 20, and 30 km s^{-1} (atmosphere G and partial redistribution). (*a*) Lβ. (*b*) Lα.

profiles, for Lβ as well as for Lα, have smoother peaks than any of the computed profiles. Furthermore, it appears very difficult to obtain a correct ratio of peak-to-central intensity for both Lβ and Lα without macroturbulence. If one tries, for instance, to obtain a good ratio for Lα by decreasing the thickness of the plateau or extending the transition region, the reversal disappears in Lβ before reaching a correct value for Lα (see model E). In the regions where the slope is smoother, the macroturbulence may not bring about important changes. For instance, it is unlikely to change the shape of the wings.

We added macroturbulence by convolving the profiles by a function representing the probability distribution of velocities. Due to the lack of information about this distribution, we assumed it to be Maxwellian and tried a set of different mean velocities for some of the profiles obtained previously. We have plotted on Figure 8 the profiles corresponding to model G assuming partial redistribution, for some macroturbulence velocities from 0 to 30 km s^{-1}. For Lβ (Fig. 8*a*), the best results are obtained, roughly, with a rms velocity of 20 km s^{-1}; for Lα (Fig. 8*b*), the value of 30 km s^{-1} seems better. The magnitude of the macroturbulent velocities required to obtain a correct fit of the observed line cores shows clearly that the microturbulent assumption is not valid in the case of the Lyman lines. A more detailed understanding of the motions in the high chromosphere is needed to account for the profiles of these lines.

VI. LINES FROM OTHER ELEMENTS

In the spectral range covered by the Lβ line, one may find several lines produced by other elements. Limiting, somewhat arbitrarily, this spectral range to 2 Å (centered at 1025.72 Å), we may expect the contributions of at least four lines produced by ionized helium, neutral oxygen, and ionized magnesium. The positions of these lines are indicated on Figure 9, with the observed profile.

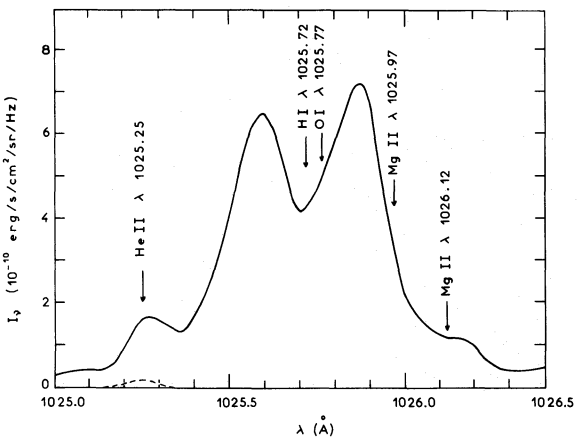

FIG. 9.—Observed Lβ profile (*full line*) with the positions of the lines from different emitters; *dashed line*, He II (2–6) profile with intensity corresponding to that of the observed (1–6) line (see text).

Let us first examine the contributions of the doublet of Mg II at 1025.97 Å and 1026.12 Å. These lines arise from the (3*s*–5*p*) transition. As long as these lines do not appear clearly on the observed spectrum, we sought an order of magnitude of their intensities by computing a somewhat oversimplified three-level and continuum atom (to take into account the Mg III/ Mg II ionization equilibrium). The abundance of the Mg II atom was estimated by assuming a LTE ratio for Mg II/Mg I (actually, Mg I is very rare in the chromosphere). The collisional excitation cross sections were taken from Blaha (1972) and the collisional ionization coefficients from Martin, Peart, and Dolder (1968); we also used the photoionization measurements by Black, Weisheit, and Laviana (1972) and the transition rates of Wiese, Smith, and Miles (1969). We computed the profiles corresponding to model A. The source functions obtained for the two lines are lower than those of Lβ, which results in very weak absorption lines. The depressions so obtained for the line centers, relative to the Lβ wing, are about 4% for the 1025.97 Å line and 6% for the 1026.12 Å line. So these lines may be neglected in practice.

The (^3P–$^3D^o$) transitions of neutral oxygen forms a triplet with a line located at 1025.77 Å, very close to the center of Lβ. The other components are outside our range, at 1027.42 Å and 1028.15 Å. The line at 1025.77 Å is responsible for a pumping process which may increase the strengths of a number of other oxygen lines (see Bowen 1947; Haisch *et al.* 1977). This line being located less than one Doppler width from the center of Lβ, its absorption coefficient may be neglected with respect to the hydrogen line (a rough approximation gives a ratio of 2×10^{-4}), and it does not influence the profile.

The case of the line of ionized helium at 1025.25 Å is somewhat different. It is an optically thin line arising from the chromosphere-corona transition region, so its emission may simply be added to the intensities in the Lβ blue wing. This line corresponds to a degenerate triplet whose subtransitions are (2*s*–6*p*), (2*p*–6*s*), and (2*p*–6*d*). This line appears on Figure 9 as a deformation of the blue wing of Lβ. We tried to compare this line with the (1–6) line (Lε) of He II, measured by Linsky *et al.* (1976). If we assume that the two lines are optically thin, their intensities are proportional to the number density of ions in the upper state, integrated along the line of sight, multiplied by $A_{ji}\nu_{ji}$ (Einstein coefficient and frequency). In this case, the ratio of intensities of the (2–6) and (1–6) lines is expected to be

$$\frac{I_{26}}{I_{16}} = \frac{\nu_{62}}{\nu_{61}} \times \frac{A_{62}}{A_{61}} \approx 0.135 .$$

The mean value for the quiet Sun given by Linsky *et al.* (1976) is $I_{16} = 45$ ergs s^{-1} cm^{-2} sr^{-1}. The corresponding value for (2–6) is thus $I_{26} \approx 6.1$ ergs s^{-1} cm^{-2} sr^{-1}. The line shape obtained from this integrated intensity, with an assumed Gaussian profile corresponding to a turbulent velocity of 15 km s^{-1} and a temperature of 10^5 K, is plotted on Figure 9.

The value so obtained is too weak to reproduce the observed deformation, by a factor of about 4; this may be explained by the fact that the (1–6) transition is perhaps not optically thin, or by the errors in our absolute calibration and that of Linsky *et al.* (1976).

VII. CONCLUSION

It seems that, for the formation of the Lyman lines of hydrogen, the solar atmosphere may be approximated by a one-dimensional model atmosphere, provided that: the microturbulent assumption would be replaced by a more accurate treatment of chromospheric motions in order to explain the cores of the lines; and the temperatures in the region under the plateau would be increased with reference to the Vernazza, Avrett, and Loeser (1973) solar model, if partial redistribution is taken into account, to produce a correct fit of the near wings.

The asymmetries of the lines, which may be seen on Figures 1*a* and 1*b*, are actually variable with time and location, and are probably related to large-scale motions of the atmosphere. Their amplitudes, however, remain low on the quiet Sun.

We wish to thank John Leibacher and Roger Bonnet for critical reading of the manuscript, Nguyen Tran-Minh, Nicole Feautrier, and Monique Malinovsky for fruitful discussions about atomic physics involved in this paper, and Andrew Skumanich and Alain Jouchoux for their help during our stay in Boulder in 1977 May. The computations were done on the computer of Centre National d'Études Spatiales, in Toulouse, under contract 77 CNES 202.

APPENDIX

COLLISION-BROADENING HALF-WIDTHS

If elastic collisions may be treated in the impact approximation and give a Lorentzian profile of half-width δ_ν^E, the redistribution functions for the Lyman lines are given by the OSC approximation. If inelastic collisions are negligible, we have

$$R_{\nu'\nu} = \gamma R^{\mathrm{II}}{}_{\nu'\nu} \quad (1-\gamma) R^{\mathrm{III}}{}_{\nu'\nu}$$

with

$$\gamma = \delta_\nu^N/(\delta_\nu^N + \delta_\nu^E)$$

(δ_ν^N, natural half-width; see Milkey and Mihalas 1973).

Unfortunately, the collisional profiles for the Lyman lines are not pure Lorentzian-impact-approximation profiles; but the OSC approximation being the only one available now, we used it and approximated real profiles by Lorentzian profiles as shown below, anticipating further theoretical corroboration of this procedure.

For resonance broadening, we used the formula of Furssow and Wlassow (reported by Breene 1961),

$$\delta_\nu^R = \frac{8\pi}{3}\frac{e^2 f}{m\omega_0} N_1$$

(f, oscillator strength; N_1, number density of hydrogen in the fundamental level; the other symbols have their usual meanings), which gives, for Lα,

$$\delta_\nu^R\,(\mathrm{Hz}) \approx 5.7 \times 10^{-8} N_1\,(\mathrm{cm}^{-3}),$$

and, for Lβ,

$$\delta_\nu^R\,(\mathrm{Hz}) \approx 9.1 \times 10^{-9} N_1\,(\mathrm{cm}^{-3}).$$

For Stark broadening in the region of interest ($N_e \sim 10^{11}$ cm^{-3}, $T_e \sim 10^4$ K, $\Delta\lambda \sim 1$ Å), the profile is equivalent to a Holtsmark profile,

$$S(\alpha) \approx S_0 \alpha^{-5/2}$$

with $\alpha = \Delta\lambda/F_0$ ($F_0 = 1.25 \times 10^{-9} N_e^{2/3}$ for $\Delta\lambda$ in angströms; see, for instance, Vidal, Cooper, and Smith 1973). The equivalent Lorentz profile, in the neighborhood of the wavelength $\Delta\lambda_0$, is:

$$\mathrm{L}(\alpha) = \frac{1}{\pi\delta\alpha}\frac{1}{1+(\alpha/\delta\alpha)^2} \approx \frac{\delta\alpha}{\pi}\alpha^{-2}$$

(for $\alpha \gg \delta\alpha$), with

$$\mathrm{L}(\Delta\lambda_0/F_0) = S_0(\Delta\lambda_0/F_0)^{-5/2},$$

which gives

$$\delta\alpha = \pi S_0(\Delta\lambda_0/F_0)^{-1/2},$$

and

$$\delta_\lambda^S = F_0\delta_\alpha = \pi S_0 F_0^{3/2}\Delta\lambda_0{}^{-1/2},$$

or, in frequency units,

$$\delta_\nu^S = (c/\lambda_0{}^2)\delta_\lambda^S.$$

Numerically, we have, for Lα,

$$S_0 \approx 6.72 \times 10^{-6}\ (\mathrm{cgs\ units}),$$

which gives, for $\Delta\lambda_0 = 1$ Å,

$$\delta_\nu^S\,(\mathrm{Hz}) \approx 1.87 \times 10^{-6} N_e\,(\mathrm{cm}^{-3}),$$

and, for Lβ, in the same way,

$$S_0 \approx 3.58 \times 10^{-5}\ (\mathrm{cgs\ units}),$$

$$\delta_\nu^S\,(\mathrm{Hz}) \approx 1.41 \times 10^{-5} N_e\,(\mathrm{cm}^{-3}).$$

The natural line width is lower for Lβ than for Lα, and the Stark width higher, so that there is a substantial amount of incoherent scattering in the wings of Lβ, whereas the Lα wings remain close to those corresponding to coherent scattering in the rest frame of the atom (R_{IIA} redistribution function of Hummer 1962) (see Fig. 10).

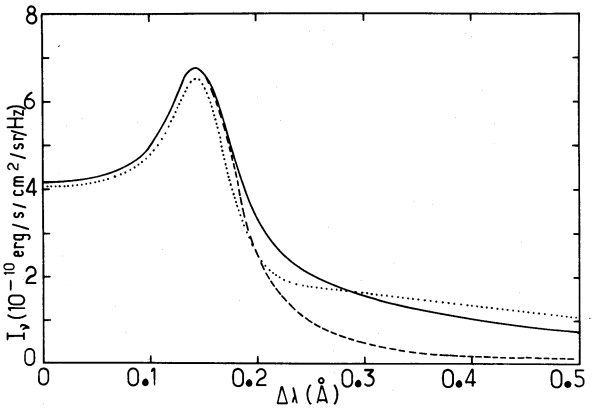

FIG. 10a

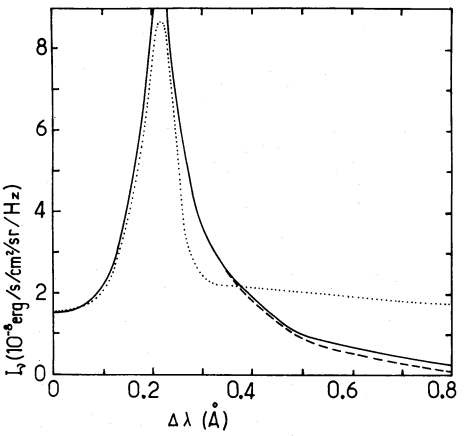

FIG. 10b

FIG. 10.—Comparison of CRD and PRD profiles (atmospheric model F). *Full line*, PRD with redistribution functions corresponding to the OSC approximation; *dotted line*, complete redistribution; *dashed line*, R_{IIA} redistribution function (scattering coherent in the rest frame of the atom). (*a*) Lα. (*b*) Lβ.

REFERENCES

Artzner, G., Bonnet, R. M., Lemaire, P., Vial, J. C., Jouchoux, A., Leibacher, J., Vidal-Madjar, A., and Vite, M. 1977, *Space Sci. Instr.*, **3**, 131.
Avrett, E. H., Vernazza, J. E., and Linsky, J. L. 1976, *Ap. J. (Letters)*, **207**, L199.
Black, J. H., Weisheit, J. C., and Laviana, E. 1972, *Ap. J.*, **177**, 567.
Blaha, M. 1972, *Astr. Ap.*, **16**, 437.
Bonnet, R. M., *et al.* 1978, *Ap. J.*, **221**, 1032.
Bowen, I. S. 1947, *Pub. A.S.P.*, **59**, 196.
Brault, J. W., and White, O. R. 1971, *Astr. Ap.*, **13**, 169.
Breene, R. G. 1961, *The Shift and Shape of Spectral Lines* (Oxford: Pergamon).
Bruns, A. V., Grechko, G. M., Gubarov, A. A., Klimuk, P. I., Sevastyanov, V. I., Severny, A. B., and Steshenko, N. V. 1976, in *IAU Colloq. No. 36*, ed. R. M. Bonnet and P. Delache, p. 333.
Cannon, C. J. 1976, *Astr. Ap.*, **52**, 337.
Cuny, Y. 1967, *Ann. d'Ap.*, **30**, 143.
———. 1968, *Solar Phys.*, **3**, 204.
Feautrier, P. 1964, *CR Acad. Sci. Paris*, **258**, 3189.
Gingerich, O., Noyes, R. W., Kalkofen, W., and Cuny, Y. 1971, *Solar Phys.*, **18**, 347.
Gouttebroze, P. 1977, *Astr. Ap.*, **54**, 203.
Haisch, B. M., Linsky, J. L., Weinstein, A., and Shine, R. A. 1977, *Ap. J.*, **214**, 785.
Hirayama, T. 1971, *Solar Phys.*, **16**, 384.
Hummer, D. G. 1962, *M.N.R.A.S.*, **125**, 21.
Jordan, C. 1975, *M.N.R.A.S.*, **170**, 429.
Lemaire, P., Charra, J., Jouchoux, A., Vidal-Madjar, A., Artzner, G., Vial, J. C., Bonnet, R. M., and Skumanich, A. 1978, *Ap. J. (Letters)*, **223**, L55.
Linsky, J. L., Glackin, D. L., Chapman, R. D., Neupert, W. M., and Thomas, R. J. 1976, *Ap. J.*, **203**, 509.
Makarova, E. A., and Kharitonov, A. V. 1969, *Soviet Astr.*, **12**, 599.
Martin, S. O., Peart, B., and Dolder, K. T. 1968, *J. Phys. B*, **1**, 537.
Mihalas, D. 1970, *Stellar Atmospheres* (San Francisco: Freeman).
Milkey, R. W., and Mihalas, D. 1973, *Ap. J.*, **185**, 709.
Nicolas, K. R., Kjeldseth Moe, O., Bartoe, J.-D. F., and Tousey, R. 1976, *J. Geophys. Res.*, **81**, 3465.
Omont, A., Smith, E. W., and Cooper, J. 1972, *Ap. J.*, **175**, 185 (OSC).
Tousey, R. 1963, *Space Sci. Rev.*, **2**, 3.
Tousey, R., Purcell, J. D., Austin, W. E., Garrett, D. L., and Widing, K. G. 1964, *Space Res.*, **4**, 703.
Vernazza, J. E. 1972, Ph.D. thesis, Harvard University.
Vernazza, J. E., Avrett, E. H., and Loeser, R. 1973, *Ap. J.*, **184**, 605.
Vidal, C. R., Cooper, J., and Smith, E. W. 1973, *Ap. J. Suppl.*, No. 214, **25**, 37.
Wiese, W. L., Smith, M. W., and Miles, B. M. 1969, *Atomic Transition Probabilities* (NSRDS-NBS 22, Vol. **2**).

G. ARTZNER, P. GOUTTEBROZE, P. LEMAIRE, and J. C. VIAL: Laboratoire de Physique Stellaire et Planétaire, P.O. Box 10, 91370 Verrières-le-Buisson, France